This article has been accepted for publication in a future issue of this journal, but has not been fully edited. Content may change prior to final publication. Citation information: DOI10.1109/JSYST.2021.3100409, IEEE Systems Journal

Allocation of Dump Load in Islanded Microgrid using the Mixed-Integer Distributed Ant Colony Optimization

Maen Z. Kreishan, Ahmed F. Zobaa, *Senior Member, IEEE*

***Abstract*—In highly penetrated microgrids, the problem of voltage and frequency deviations exceeding their permissible limits, becomes significant with higher share of renewable based distributed generation. The existing real-time control systems of highly penetrated microgrids cannot cope on its own with such deviations, owing to the large generation and demand mismatch mainly during off-peak hours. A dump load can help with voltage and frequency regulation by consuming excess generation. However, further investigation is required to highlight the importance of optimal dump load allocation on the operation of microgrids. The mixed-integer distributed ant colony optimization is introduced as a novel application in droop controlled islanded microgrids to minimize voltage and frequency deviations and system losses. The optimization problem was formulated as a single- and multi-objective problem to allocate a dump load and the optimal droop settings for distributed generation in islanded microgrid during off-peak hours. The proposed optimization method was teamed up with a special backward/forward sweep load flow method to account for distributed generation droop characteristics and enhance the solution convergence. The method was applied to the IEEE 69- and 118-test systems and validated against competitive swarm and evolutionary metaheuristics. Results have shown that an optimally sized and allocated dump load with optimized droop setting could minimize voltage and frequency deviations to an acceptable level, while reducing power losses incurred by the installation of such load into the microgrid.**

Index Terms- Ant Colony Optimization, Backward/Forward Sweep, Droop Control Islanded Microgrid, Dump Load, Multi-objective Optimization

NOMENCLATURE

f_0, f, f_{ss}	Nominal, operating and steady state frequency
V_0, V_i	Nominal and operational voltage at bus i
P_{Gi0}, P_{Gi}	Nominal and generated active power at bus i
Q_{Gi0}, Q_{Gi}	Nominal and generated reactive power at bus i
m_{pi}, n_{qi}	Frequency and voltage droop coefficients at bus i
m_{pT}, n_{qT}	Equivalent frequency and voltage droop coefficients
mn_{DL}	Optimum droop settings for dump load allocation
P_{Li}, Q_{Li}	Active and reactive power consumed by load at bus i
P_{Li0}, Q_{Li0}	Load's active and reactive power at nominal voltage
nP, nQ	Load's voltage dependence coefficients
F_p , F_q	Load's frequency dependence coefficients
P_{DL}, Q_{DL}	Active and reactive power consumed by dump load
gk, lk	Total number of DG units and loads in MG
$\mathcal{N}$	Set of all system buses
$\mathcal{GK}$	A subset containing all DG buses
P_{loss}, Q_{loss}	Total active and reactive losses of the MG
Δf, ΔV_i	Frequency and voltage deviations at bus i
E, ε_{Th}	Tolerance and threshold values for convergence criteria
c_1, c_2	Load flow method iteration counters
S_i, I_i	Apparent power and current injects at bus i
B_i	Branch current flowing from bus i to bus $i+1$
B_{i_max}	Maximum limit for branch current B_i
V_{in}	New voltage value for bus i at iteration c_1
Z_i, R_i, X_i	Impedance, resistance and reactance of branch B_i
f_{c_2+1}, f_{c_2}	Frequency at the c_2+1 and c_2 iterations
$V_{1_{c_2+1}}$, $V_{1_{c_2}}$	Voltage at the c_2+1 and c_2 iterations
U_i, N_i	The Utopia and Nadir of an objective function
$f_i(x)$	The objective function
x	Decision variable of the problem.
w_i^j	Matrix of weights for each sub-problem
$d_i^j(x)$, $D_j(x)$	Solution x weighted and average distance
$B_j(x)$	The balance function
$T_j(x)$	The target function
$\mathcal{O}$, $\mathcal{C}$	Total number of objectives and constraints
$g_i(x)$	The constraints handling function
$\mathcal{C}_e$	The number of equality constraints

I. INTRODUCTION

DEVELOPMENTS in distributed generation (DG) design and control has brought forward the concept of microgrids (MGs) operation. MGs could bring considerable benefits to the environment, the economy and energy supply security. However, with such benefits more technical and operational challenges arise from modelling, operating, and maintaining MGs [1]. The ability of MGs to operate independently from utility grid could increase supply reliability while minimizing the cost for consumers and network operators, this type of operation is called autonomous or islanded MGs (IMGs) [2]. During grid-connected mode variations in bus voltage (V) and operating frequency (f) due to moderate generation/load mismatches are dealt with by utilities' main control schemes in real-time. However, the issue become complex in islanded mode with higher probability of large mismatch especially during off-peak hours. The probability of such situation increases by the intermittent nature of variable renewable generation.

Integration of variable renewable resources mainly wind power and solar photovoltaics in modern power grids has significantly increased in the last decade [3]. This has resulted in considerable challenges mainly: the inability of existing generation to meet load demand at all times, and transmission capacity inadequacy to accommodate excessive renewable generation [4]. According to the German, Italian and British grids currently facing high renewables penetration, this continued renewable growth will lead to future V-f regulation issues [3]. Therefore, an efficient power management solution must be implemented in real-time for MGs with high penetration of dispatchable and non-dispatchable renewable generation. Different power management strategies were suggested by [5]–[11]

This article has been accepted for publication in a future issue of this journal, but has not been fully edited. Content may change prior to final publication. Citation information: DOI10.1109/JSYST.2021.3100409, IEEE Systems Journal

which include: the utilization of battery energy storage systems (BESS) to store extra power at off-peak hours, coordinated smart charging techniques of electric vehicles (EV), demand response (DR) management, and employing an electronic load controller (ELC) with dump load (DL) or smart load to consume excess generation at off-peak hours. There are some economic, environmental, and technical barriers that hinder the use of extra BESS to help with excess power generation at off-peak hours [12]. Moreover, the use of DR and EV smart charging techniques to regulate microgrid power variations does not always return the desired effect due to behavioural and coordination issues [13]. As a result, ELC controlled DL has gained significant interest to assist with wind and hydro power control problems for synchronous and asynchronous units deployed in IMGs [14]–[17]. The use of DL in microgrids proved to be a good solution to maintain the flow of existing power and thus achieve V-f regulation while dissipating the excessive power as heating or pumping applications [18], [19]. However, the use of ELC is still at the developing stage in IMGs, as generator thermal strain and power wastage were identified as shortcomings to further deployment of DL in MGs [17]. Hence planning studies to expand the use of ELC loads in IMG are of vital importance for V-f regulation.

To achieve V-f regulation during islanding operation different control strategies are selected to manage IMGs, most predominant strategies are the master-slave and droop control which can be found at [20] and [21] respectively. In droop control method the active power (P) and reactive power (Q) output of DG units become a function of the f and V of the system respectively. This is due to the (P-f) and (Q-V) droop settings assigned to the DG units by the power electronics interfaces which facilitate load sharing between all DG units during islanding [22]. This type of IMG is referred to as droop controlled islanded MG (DCIMG). The area of optimal operation of DCIMG has attracted the attention of researchers in recent years but has not yet been fully addressed in literature. The location and droop settings for DG units have been optimized in DCIMG with different goals: net energy export maximization [23], small signal stability and power loss minimization [24], minimize generation costs and improve voltage profile [25], [26]. Nonetheless, studies [23]–[26] had no account for V-f deviations at off-peak hours and did not propose a way to implement power management solutions in DCIMG. To accommodate trending power management solutions in DCIMG, studies [27]–[30] focused on the optimal allocation of BESS with the aim of minimizing costs and reducing emissions. Despite the promising economic and environmental outcomes of these studies, no solutions were proposed to address the inherited efficiency problems of increasing the number of BESS in MGs. To address problems arising from increased BESS use in DCIMG and power imbalance at off-peak hours in highly penetrated MGs, an optimal allocation study of ELC was proposed in [31]. However, [31] had some limitations in the algorithm computational run time which makes it less reliable in real-time application, no consideration of active and reactive losses caused by DL installation, and the effect of droop characteristics on the solution was not taken into account. Furthermore, limited number of iterations were allowed for droop control in the proposed algorithm due to convergence issues for the suggested load flow method called direct backward\forward sweep (DBFS) proposed by [32]. Those convergence issues arise from the tolerance value of voltage fluctuations determining the criteria for the DBFS convergence, which were further highlighted by [33]. In real-life problems, convergence of the solution for non-convex mixed-integer non-linear problems (MINLPs) is of great importance. Different swarm and evolutionary algorithms were proposed to optimize DCIMG operation [23]–[31]. The main algorithms were: the particle swarm optimisation (PSO) and the genetic algorithm (GA) as well as their variations for multi-objective problems. Despite the advantages of these methods in finding feasible non-dominated solution, they still suffer from limitation of heuristic methods and the computational burden that follows them. The search is still ongoing for new efficient algorithms and their applications to solve real life non-convex MINLPs [34], [35]. Ant colony optimization (ACO) metaheuristic is a group of algorithms influenced by ant colonies' food search behaviour in nature to serve the purpose of discrete optimization [36]. However, these algorithms have been expanded further in literature to tackle several MINLPs [34] as well as multi-objective ACO (MOACO) [37]. The proposed algorithm however has been developed by combining the extended ACO [34] with the oracle penalty method (OPM) [38] to solve multi-objective MINLPs. It differs from ordinary MOACO algorithms by its' utopia-nadir information approach to balance the solution search space on an area of interest at the Pareto front (see Schluter *et al.* [39], [40]).

In the view of the forgoing literature survey, it is concluded that, increasing BESS number and reliance on DR alone to sort out excess generation problem in highly penetrated DCIMG is costly and inefficient. DL could provide solution to the problem but only one study considered such attempt without account for optimization algorithm speed and accuracy. Also, impact on system losses and optimal droop settings were not considered. In this paper, a novel methodology has been proposed to address limitations of previous studies by formulating the single- and multi-objective optimization problem to minimize V-f deviations and power losses. We propose using a special BFS (SBFS) load flow method along with mixed-integer distributed ant colony optimization (MIDACO) to find new optimal location and size for the DL in DCIMG while obtaining an optimum droop setting for the DG units on IEEE 69- and 118-bus systems.

This paper is organised as follows: In Section I, a background of V-f regulation problem in DCIMC is introduced. Section II, the methodology development has been explained and network models used for the study were also described. Section III, the problem formulation in three stages is explained in three cases: 1) obtain single objectives problems only (min ΔV, min Δf), 2) obtain ΔV and Δf as two-objectives problem, 3) four-objectives problem (min ΔV, min Δf, min P_{loss}, and min Q_{loss}) were obtained as many-objectives problem. The last two sections IV and V, demonstrate discussion of results obtained and the conclusion respectively.

II. METHODLOGY

In this section the methodology is divided and explained in three sections: droop control method, special BFS load flow method, and proposed optimization method.

This article has been accepted for publication in a future issue of this journal, but has not been fully edited. Content may change prior to final publication. Citation information: DOI10.1109/JSYST.2021.3100409, IEEE Systems Journal

A. Droop control method and distribution network models

According to the IEEE std. 1547.4, islanding mode could be allowed if an appropriate V-f control strategy was adopted [41]. This will enable DG units to account for load changes without relying on external power supply. A complete control strategy of IMGs is often implemented in hierarchal levels: primary level droop control, secondary level control loop to restore nominal V-f by vertically shifting droop curves and tertiary level control using a microgrid central controller (MGCC) to monitor and optimize the IMG performance in real-time [30]. The latter level influences the implementation of the optimization cycles in real-time, and is usually carried out ahead of time up to 15 mins before load and generation forecast. The proposed optimization method could be adopted by MGCC to analyse forecasted data, and the optimal solution is fed to DL and DG units by low bandwidth communication channels. Tertiary control and generation/load forecast require an independent study, hence will not be covered in this paper and shall be the focus of future work.

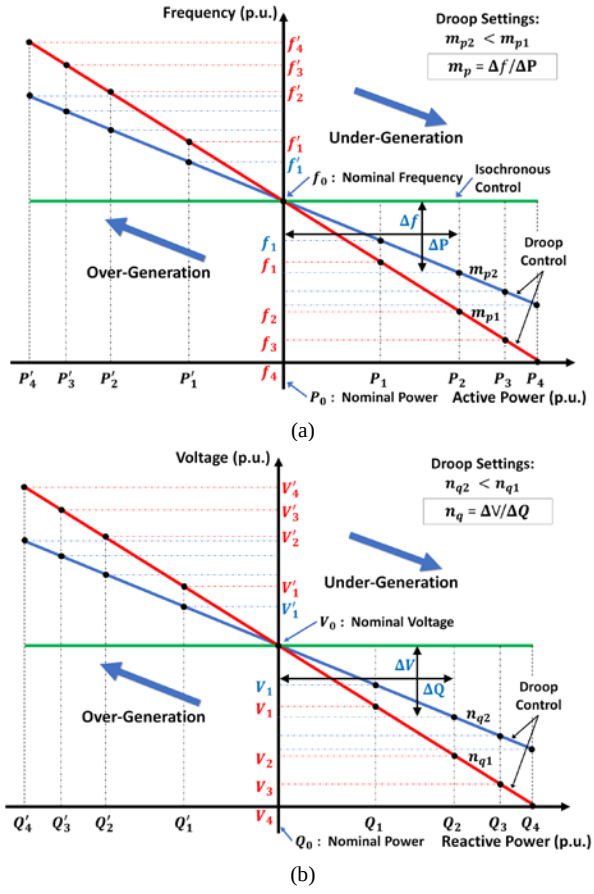

Fig. 1. Droop characteristics of DG units (a) P-f droop (b) Q-V droop

The DG model selected for this study is of inverter-based DG type (IBDG) where power electronics facilitate V-f droop control. The P-f and Q-V droop equations in (1) and (2) respectively, were incorporated in the inverter control system. This will allow DG units to respond to load variations in the IMG as per IEEE std.1547.7 requirements [33], [42]:

$$f - f_0 = m_{pi}\,(P_{Gi} - P_{Gi0}) \quad (1)$$

$$|V| - |V_0| = n_{qi}\,(Q_{Gi} - Q_{Gi0}) \quad (2)$$

TABLE I
DG UNITS DROOP GAINS

DG Unit	DG_1	DG_2	DG_3	DG_4	DG_5	DG_6	DG_7	DG_8
m_{pi}	-0.05	-1	-0.1	-1	-0.2	-1	-0.1	-1
n_{qi}	-0.05	-1	-0.1	-1	-0.2	-1	-0.1	-1
Bus No. 69-bus System	1	6	15	30	55	-	-	-
Bus No. 118-bus System	1	20	39	47	73	80	90	110

The rate at which a DG unit contributes to power variations of the MG is called the droop coefficient, meaning that a DG unit with smaller absolute droop coefficient value contribute more to the load demand change. The pre-defined droop coefficients selected for this study are obtained from [31]–[33] and shown in Table I. The P-f and Q-V droop characteristics of a typical DG unit are shown in Fig. 1. When generation exceeds demand, the DG active power decreases from P_0 to P_4' to suppress frequency rise where it settles at f_4' (Fig. 1(a)). As for DG reactive power output and demand variations shown in Fig. 1(b), in case of over-generation situation, the reactive power output will decrease from Q_0 to Q_4', thus DG bus voltage will settle at V_4' above V_0. It should be noted though that the values of (P_4') and (Q_4') should not exceed the rated power of the unit, otherwise, DG units must be set to constant PQ control. The update of active power and frequency occurs in an iterative or steps process. Meaning, in over-generation situation step 1 (f_0, P_0) to (f_1', P_1') then step 2 (f_1', P_1') to (f_2', P_2') and so on. The same applies to reactive power and voltage updates, i.e. step 1 (V_0, Q_0) to (V_1', Q_1') then step 2 (V_1', Q_1') to (V_2', Q_2') and so on. Static load models describe the dependency of load active and reactive power as function of the system V-f at one specific instant of time. This can be expressed mathematically in the following equations [43]:

$$P_{Li} = P_{Li0}\left(\frac{|V_i|}{|V_0|}\right)^{nP}\left(1 + (f - f_o)\,.F_p\right) \quad (3)$$

$$Q_{Li} = Q_{Li0}\left(\frac{|V_i|}{|V_0|}\right)^{nQ}\left(1 + (f - f_o)\,.F_q\right) \quad (4)$$

Naturally, loads consist of static and dynamic components which are derived from the nature of the load whether it was residential, commercial, or industrial. The coefficients selected to represent the load model used for this study are shown in Table II [33]. As for the DL model used, it follows the static load model selected to represent the loads for this study. Further information about the design and operation of the ELC in MGs can be found in studies [14]–[19]. Almost all installations of DL in literature were located at the main generator bus. However, in this study the location of DL can be random satisfying certain criteria and could be away from a generating bus. The following equilibrium equations (5) and (6) must hold in the system upon the installation of DL into the MG:

$$\sum_{i=1}^{gk} P_{Gi} = \sum_{i=1}^{lk} P_{Li} + P_{DL} + P_{loss} \quad (5)$$

$$\sum_{i=1}^{gk} Q_{Gi} = \sum_{i=1}^{lk} Q_{Li} + Q_{DL} + Q_{loss} \quad (6)$$

TABLE II
STATIC LOAD MODEL V-F COEFFICIENTS

Static Load Type	Setting	nP	nQ	F_p	F_q
Constant Power Load	Set 1	0	0	0	0
V-f Dependent load	Set 2	2	2	1	1

This article has been accepted for publication in a future issue of this journal, but has not been fully edited. Content may change prior to final publication. Citation information: DOI10.1109/JSYST.2021.3100409, IEEE Systems Journal

B. *Special BFS load flow method*

There are many load flow methods available in literature, such as: Newton-Raphson, Gauss-Seidel, BFS, etc. [33]. Nevertheless, most of these methods are not suitable for power flow studies in DCIMGs. This is attributed to the absence of frequency as a variable, the high R/X ratio of distribution networks and the need to obtain the computationally expensive Jacobean matrix. Therefore, different variations of the BFS methods have been proposed to solve load flow in DCIMG [32], [33]. In this paper, a combination of DBFS [32] and modified BFS (MBFS) [33] has been used to perform load flow calculations for DCIMG by eliminating the convergence issues of both methods. The main difference between proposed SBFS and the previous two methods is summarized as follows:

- Removal of the additional frequency update loop suggested by DBFS and adopting higher tolerance voltage update solely as the convergence criteria.
- Restricting the active and reactive power change at the update stage only rather than twice at the backward sweep and at the update stages as reported by MBFS.
- Elimination of second matrix subroutine for the voltage matrix in contrary with DBFS and MBFS where two subroutines were required to obtain two matrices for current and voltage.

The proposed SBFS consists of four parts: initialization stage, backward sweep, forward sweep and the update stage:

1) *Initialization stage*

A bus is selected to act as a virtual bus (VB) which mimic the behaviour of pseudo-grid. In this paper, bus 1 was selected to act as VB. An initialisation process starts by setting all system voltages V_i to $1\angle 0^{\circ}$ p.u.; Δf, ΔV_1 to zero; reset iteration counters c_1 and c_2; determine voltage tolerance threshold $\varepsilon_{Th} = 10^{-8}$, DG units droops and loads coefficients.

2) *Backward sweep*

From this stage, the voltage is known at each bus so are the pre-islanding active and reactive powers of DG units and loads, so we procced with calculating apparent power using (7) and then current injects at each bus moving backward towards the VB using (8).

$$S_i = (P_{Li} - P_{Gi}) + j(Q_{Li} - Q_{Gi}) \quad (7)$$

$$I_i = \left(S_i / V_i\right)^* \quad (8)$$

To obtain the current in each branch of the system using (9), the branch-inject branch-current matrix ($BIBC$) must be created first as instructed in [44].

$$[\boldsymbol{B_i}] = [\boldsymbol{BIBC}][\boldsymbol{I_i}] \quad (9)$$

Where $[\boldsymbol{B_i}]$ and $[\boldsymbol{I_i}]$ are single column matrices of branch and inject currents respectively. For a radial system of n buses and m branches $[\boldsymbol{BIBC}]$ is an m by $n-1$ matrix consisting of $zeros$ and $ones$ as defined in [44].

3) *Forward sweep:*

At this stage, new values for voltages across the system are calculated using (10), while the voltage tolerance value E for convergence criteria is calculated using (11):

$$[\boldsymbol{V_{in}}] = [\boldsymbol{V_1}] - [\boldsymbol{BCBV}][\boldsymbol{B_i}] \quad (10)$$

$$\mathrm{E} = \max |V_{in} - V_i| \quad (11)$$

$$[\boldsymbol{BCBV}] = [\boldsymbol{BIBC}]^T \odot \left[[\boldsymbol{1}][\boldsymbol{Z_i}]\right] \quad (12)$$

Where $[\boldsymbol{BCBV}]$ is the branch current and bus voltage matrix obtained by the simple matrix manipulation of (12) contrary with DBFS and MBFS; T and $\odot$ are matrix operators for transpose and Hadamard product respectively; for a radial distribution system with n buses $[\boldsymbol{1}]$ is a $ones$ vector matrix of size $(n-1)$ x 1; $[\boldsymbol{Z_i}]$ is a 1 x $(n-1)$ row vector of impedance Z_i.

4) *The Update stage:*

If the tolerance value is smaller than that of ε_{Th}, then new values of frequency and voltage are obtained according to (13) and (14):

$$\Delta f = -m_{pT} \cdot (P_{G1} - \Re\{V_1 \cdot B_1^*\}) \quad (13)$$

$$\Delta V_1 = -n_{qT} \cdot (Q_{G1} - \Im\{V_1 \cdot B_1^*\}) \quad (14)$$

Where m_{pT} and n_{qT} are the equivalent f and V droop coefficients of the system respectively, and given by:

$$m_{pT} = \left(\sum_{i\in\mathcal{GK}}^{gk} m_{pi}^{-1}\right)^{-1} \quad (15)$$

$$n_{qT} = \left(\sum_{i\in\mathcal{GK}}^{gk} n_{qi}^{-1}\right)^{-1} \quad (16)$$

After frequency change, the line impedance is updated as in (17), while the voltage update is reflected upon the solution by another forward sweep. Subsequently, post islanding DG output powers are updated using (18) and (19).

$$Z_i = R_i + \mathrm{j}\, X_i\left(f_{c_2+1}/f_{c_2}\right) \quad (17)$$

$$P_{Gi} = \Delta f / m_{pi} + P_{Gi0}\ ;\ \forall\, i \in \mathcal{GK};\ \mathcal{GK} \subseteq \mathcal{N} \quad (18)$$

$$Q_{Gi} = \Delta V_i / n_{qi} + Q_{Gi0}\ ;\ \forall\, i \in \mathcal{GK} \quad (19)$$

Lastly, load power is updated using (3) and (4) while losses are obtained as in (20) and (21) using an updated version of B_i just before the final verification of convergence by comparing $|\Delta V_1|$ to ε_{Th}:

$$P_{loss} = \sum_{i=1}^{n-1} \Re\{Z_i\} \cdot |B_i|^2 \quad (20)$$

$$Q_{loss} = \sum_{i=1}^{n-1} \Im\{Z_i\} \cdot |B_i|^2 \quad (21)$$

A flow chart of the proposed SBFS is depicted in Fig. 2

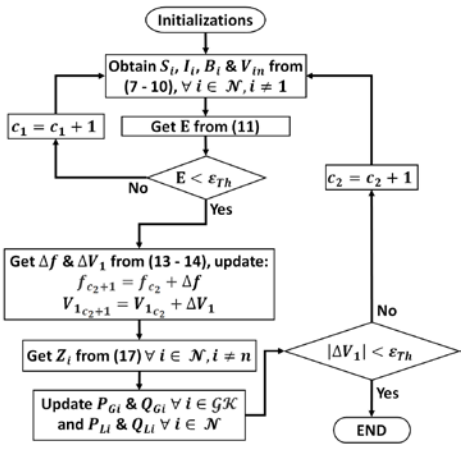

Fig. 2. Proposed SBFS flow chart

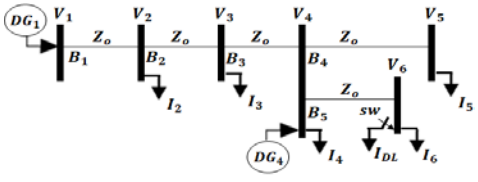

Fig. 3. 6-bus radial MG system

This article has been accepted for publication in a future issue of this journal, but has not been fully edited. Content may change prior to final publication. Citation information: DOI10.1109/JSYST.2021.3100409, IEEE Systems Journal

C. Mathematical Validation

To study the impact of DL allocation on an MG mathematically, a 6-bus radial system was depicted in Fig. 3. Bus 1 was considered the VB and modelled as droop bus where f and V_1 are updated according to m_{p1} and n_{q1} droops respectively. While bus 4 is considered as constant PQ bus in a significant over-generation situation. Based on that, the apparent power injected by $DG_1$is given as $S_{G1} = P_{G1} + jQ_{G1}$, while the total complex power injected by DG_4 is given as $S_{G4} = P_{G4} + jQ_{G4}$ such that $S_{G4} > S_{G1}$. It is assumed that the system is lossless ($Z_o \approx 0$) with balanced and identical load distribution except for bus 1, where each load complex power is given by $S_L = P_L + jQ_L$. Furthermore, it is also assumed that the load flow converges at the first iteration and that switch (sw) is left open. Denoting positive for consumed power and negative for generated power and by applying Kirchhoff's current law sweeping backward towards the VB, we have:

$$B_1 = I_2 + I_3 + I_4 + I_5 + I_6 \quad (22)$$

Substituting (22) in equation (8) we rewrite (22) as:

$$B_1 = \sum_{i=2}^{6}(S_i/V_i)^* \quad (23)$$

Since we have assumed a flat start with lossless system, then the voltage become a global variable similar to the frequency i.e. $|V_1| = |V_i| = 1$. Now, taking the high generation situation into consideration, we have $S_{G4} \gg S_{L4}$. Therefore, equation (23) becomes:

$$B_1 = 4(S_L)^* - (S_{G4})^* \quad (24)$$

Going forward sweep for the system in question the f and V_1 are updated by compensating (24) in equations (13) and (14):

$$\Delta f = -m_{p1} \cdot (P_{G1} + P_{G4} - 4P_L) \quad (25)$$

$$\Delta V_1 = -n_{q1} \cdot (Q_{G1} + Q_{G4} - 4Q_L) \quad (26)$$

Now, if sw is closed, then B_1 becomes B_1' after the inclusion of DL into the system at bus 6 and equation (22) becomes:

$$B_1' = I_2 + I_3 + I_4 + I_5 + I_6 + I_{DL} \quad (27)$$

Likewise, usually in DL application the size of such load must be considerably large to consume excess generation. Substituting (27) in (8), we have B_1' as in (28) noting that $B_1' > B_1$:

$$B_1' = 4(S_L)^* - (S_{G4})^* + (S_{DL})^* \quad (28)$$

Similarly, the f and V_1 updates upon DL connection becomes:

$$\Delta f' = -m_{p1} \cdot (P_{G1} + P_{G4} - 4P_L) + m_{p1} \cdot (P_{DL}) \quad (29)$$

$$\Delta V_1' = -n_{q1} \cdot (Q_{G1} + Q_{G4} - 4Q_L) + n_{p1} \cdot (Q_{DL}) \quad (30)$$

Since m_{p1} and n_{q1} are negative, we rewrite (29) and (30) as:

$$\Delta f' = \Delta f + m_{p1} \cdot (P_{DL}) \quad (31)$$

$$\Delta V_1' = \Delta V_1 + n_{p1} \cdot (Q_{DL}) \quad (32)$$

From (29)-(32), it is clear that $|\Delta f'| < |\Delta f|$ also $|\Delta V_1'| < |\Delta V_1|$ satisfying the assumption that V-f deviations are minimized as a result of DL application into the MG of Fig. 3.

D. Proposed Optimization Method

The proposed approach to solve the single- and multi-objective optimization problem is based on the MIDACO algorithm which acts as a general-purpose solver. This high-performance solver is based on the extended ACO algorithm (ACOmi) [34] mixed with a universal penalty method called OPM for constraints handling [38]. For the single-objective problem, MIDACO uses a probabilistic choice for constructing solutions based on multi-kernel gaussian probability density function (PDF) rather than using a pheromone table as in the original ACO metaheuristic [34]. The Gaussian PDF (GPDF) consists of several one-dimensional weighted sum of the Gaussian function. Further information about the calculations of GPDF used in the single-objective problems of MIDACO can be found in [34] and [45]. The internal GPDF of the algorithm generates samples of ANTS (N_{pop}) within a number of KERNELS (k_r) to evaluate the objective function and store it in a solution archive [46]. In constrained problems MIDACO introduced a parameter called ORACLE (Ω) which can be given by the user to estimate a close value to the objective function, more about the OPM can be found in [38]. In addition, MIDACO introduced ACCURACY parameter to fine tune any constraints violation, while SEED parameter dictates the initial seed for sampled numbers by the pseudo random-number generator [46].

As for the multi-objective optimisation handling by MIDACO, a decomposition approach is used to break the original multi-objective problem into a set of single-objective problems evaluated in serial or parallel modes [46]. The decomposition approach of MIDACO is inspired by the utopia-nadir balance concept. The utopia (U_i) is a measure of the best global minima of an individual objective function $f_i(x)$ and is given by (24) [40]:

$$U_i = min\{f_i(x) \; \forall \; x \in \mathbb{F}\} \quad (33)$$

While the nadir (N_i) on the other hand as given in (34) corresponds to worst value of $f_i(x)$ for all x solutions that belongs to a utopia U_k of an objective function $f_k(x)$ [40].

$$N_i = max\{f_i(x) \; \forall \; x : \; \exists \; k \neq i : \; f_k(x) = U_k\} \quad (34)$$

For a multi-objective problem consisting of M decomposed single-objective sub-problems. Using (33) and (34) and denoting j for a decomposed sub-problem then the weighted distance $d_i^j(x)$ and average distance $D_j(x)$ for the optimal solution x in each $f_i(x)$ are given by (35) and (36) respectively [40]:

$$d_i^j(x) = w_i^j \cdot \left(\frac{f_i(x) - U_i}{N_i - U_i}\right) \quad (35)$$

$$D_j(x) = \frac{\sum_{i=1}^{M} d_i^j(x)}{M} \quad (36)$$

Based on (26) and (27) the balance concept, $B_j(x)$, is introduced to indicate the average distance of a solution x to it's corresponding utopia and nadir values of each sub-problem [40], [46].

$$B_j(x) = \sum_{i=1}^{M} \left| d_i^j(x) - D_j(x) \right| \quad (37)$$

The purpose of $B_j(x)$ is to concentrate the search effort of MIDACO algorithm to the central part of the pareto front, where the best equally traded-off solution for all objectives exists [40], [46]. The balance concept is incorporated in MIDACO as the BALANCE parameter, where varying the value of BALANCE will change the advantage of certain objective over the others [46]. This parameter will expedite the process of reaching the optimal solution x, signalling a speed advantage of MIDACO algorithm [46]. To reconstruct the multi-objective

This article has been accepted for publication in a future issue of this journal, but has not been fully edited. Content may change prior to final publication. Citation information: DOI10.1109/JSYST.2021.3100409, IEEE Systems Journal

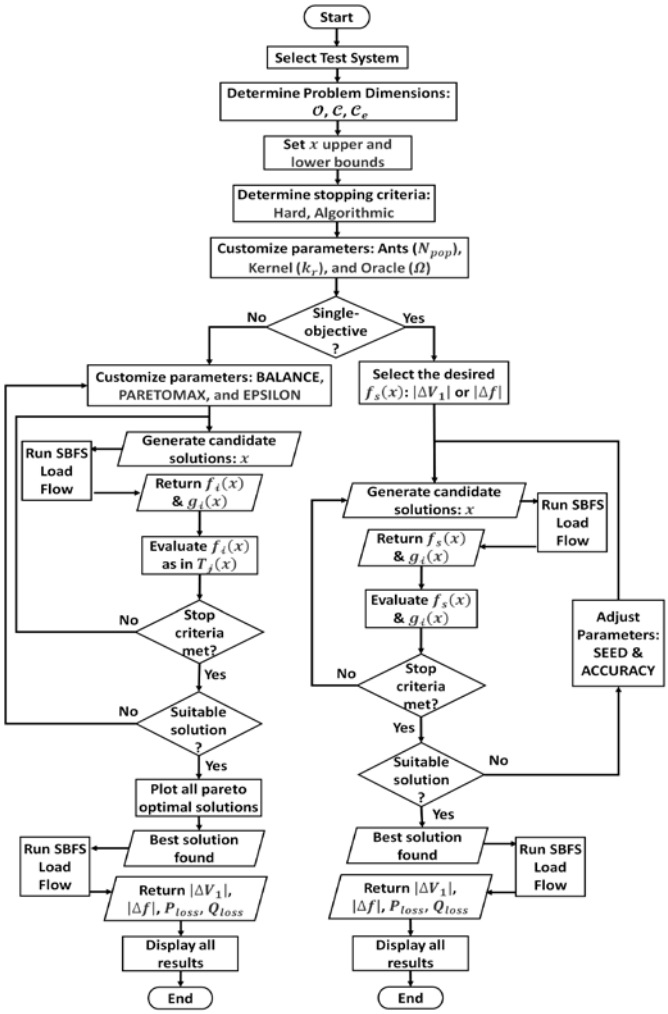

Fig. 4. Proposed optimization method flowchart

problem again for each j sub-problem, a target function $T_j(x)$ is defined in (38) to solve the original problem [40]:

$$T_j(x) = \sum_{i=1}^{M} d_i^j(x) + B_j(x) \quad (38)$$

To further fine tune the use of the BALANCE parameter, two parameters PARETOMAX and EPSILON were introduced by MIDACO [46]. The additional two parameters influence the number of non-dominated solutions on the pareto front. Where PARETOMAX limits the number of pareto points, and EPSILON sets the accuracy of pareto points filtration. A flowchart of the proposed optimization method is depicted in Fig. 4.

III. OPTIMIZATION PROBLEM FORMULATION

The optimization problem considered in this paper can be represented mathematically as:

Minimize: $\{f_i(x)\},\ i = \{1,2,\dots,\mathcal{O}\}$

Subject to: $g_i(x) = 0,\ i = \{1,2,\dots,\mathcal{C}_e\}$

$g_i(x) \geq 0,\ i = \{\mathcal{C}_e + 1,\dots,\mathcal{C}\}$

$x_{min} \leq x \leq x_{max}$

A. Objective functions

There are four objective functions in total presented in this paper:

$$f_i(x) = \begin{cases} f_1(x) = |\Delta V_1| \\ f_2(x) = |\Delta f| \\ f_3(x) = P_{loss} \\ f_4(x) = Q_{loss} \end{cases}, x = \{P_{DL}, Q_{DL}, mn_{DL}, Bus\ No.\} \quad (39)$$

However, the problem has been divided into three separate problems to see how the overall application of DL into DCIMG develops as problem dimension evolve.

1) *First problem*

A single-objective problem to obtain optimal size and location of DL by minimizing each V-f deviations at off-peak hours. Note that for the single-objective problem, the objective function can have only one value at a time denoted as $f_s(x)$:

$$f_s(x) \in \{f_1(x), f_2(x)\},\ x = \{P_{DL}, Q_{DL}, Bus\ No.\} \quad (40)$$

2) *Second problem*

A multi-objective problem to obtain optimal size and location of DL to minimize V-f deviations simultaneously takes the form:

$$f_i(x) = \{f_1(x), f_2(x)\},\ x = \{P_{DL}, Q_{DL}, Bus\ No.\} \quad (41)$$

3) *Third problem*

A many-objectives problem was formulated to obtain the optimal size and location of DL as well as optimal DG droop settings to minimize V-f deviations and network losses simultaneously takes the form:

$$f_i(x) = \{f_1(x), f_2(x), f_3(x), f_4(x)\},$$
$$x = \{P_{DL}, Q_{DL}, mn_{DL}, Bus\ No.\} \quad (42)$$

B. Constraints

The first two problems were subject to the following constraints (all numerical values were given in per-unit system with system base 12.66 KV and 11KV for 69- and 118-bus systems respectively, 500 KVA for both systems and $f_o = 50\ Hz$):

Bus voltage limit constraints:

$$0.95 \leq |V_i| \leq 1.05 \quad (43)$$

Thermal limit constraints for branch current B_i:

$$|B_i| \leq |B_{i\_max}| \quad (44)$$

DL size limits as instructed in [31]:

$$0.002 \leq P_{DL} \leq 1 \quad (45)$$

$$0.002 \leq Q_{DL} \leq 1 \quad (46)$$

As for the third problem, in addition to all previous constraints, a min-max droop settings limit has been imposed. Moreover, limiting all DG units active and reactive generation to a min-max limit. This limit must be sufficient to ensure autonomous operation of the MG without compromising on DG safe operating regions with lagging power factor (PF) values between (0.8 – 1). Furthermore, in compliance with IEEE std.1547.4 for acceptable frequency tolerance, an operating frequency limit constraint has been imposed.

$$0 \leq P_{DG} \leq 2 \quad (47)$$

$$0 \leq Q_{DG} \leq 2 \quad (48)$$

$$0.996 \leq f \leq 1.004 \quad (49)$$

Note that for the third problem a similar value denoted as mn_{DL} has been proposed for both m_{pi} and n_{qi} such that: $mn_{DL} = m_{pi} = n_{qi},\ \forall\ i \in \mathcal{GK}$, since values beyond that range would sound unrealistic [25].

$$10^{-4} \leq mn_{DL} \leq 1 \quad (50)$$

This article has been accepted for publication in a future issue of this journal, but has not been fully edited. Content may change prior to final publication. Citation information: DOI10.1109/JSYST.2021.3100409, IEEE Systems Journal

IV. RESULTS AND DISCUSSION

The MG systems chosen for this study are the IEEE 69- and 118-test systems which were modified for autonomous operation to install DG units at locations illustrated by Fig. 5. The IEEE 69- and 118-test systems parameters were taken from [47] and [48] respectively, while the DG locations and ratings were obtained from [31] and [49] for the IEEE 69- and 118-bus respectively. Systems generation/load states are illustrated in Table III, without loss of generality, each of the four scenarios demonstrate a highly probable mismatch occurrence in a highly penetrated MG. However, to generate a multi-scenario mismatch to cover all possible seasonal weather and load behaviour changes, that requires a stochastic scenario-based model of uncertainties which is beyond the scope of this paper and will be covered in future work. Four scenarios in total were adopted in this paper, scenario 1 was obtained from [31]–[33], while scenarios 2-4 were derived from [50]. It is also assumed, that the load and generation diurnal states are weakly correlated events and should not affect the outcome, hence their correlations have been neglected from the selected scenarios [50]. Simulations were carried out in MATLAB® environment with system specifications: Intel core i7 9th Generation, 2.60 GHz, and 8 GB RAM. The selected values for parameters N_{pop}, k_r and Ω were kept at default to allow the algorithm to adjust as per the convexity of the problem. This way the algorithm will dynamically change the number of N_{pop} per default number of k_r at an initial Ω value of 10^9 as the solution alternates between the feasible and unfeasible regions [46]. Moreover, for the sake of brevity, only scenario 1 from the 69-bus system was adopted for the first and second problems implementation.

A. Single Objective Optimization

TABLE III
TEST SYSTEMS GENERATION TO LOAD STATES

Scenario	Load (%)	69-Bus System		118-Bus System		Generation (%)	69-Bus System		118-Bus System	
		$\sum P_{Li}$ (p.u.)	$\sum Q_{Li}$ (p.u.)	$\sum P_{Li}$ (p.u.)	$\sum Q_{Li}$ (p.u.)		$\sum P_{Gi}$ (p.u.)	$\sum Q_{Gi}$ (p.u.)	$\sum P_{Gi}$ (p.u.)	$\sum Q_{Gi}$ (p.u.)
-	100	7.60	5.39	45.42	34.08	100	8	6	43.24	32.43
1	50	3.80	2.69	22.71	17.04	63.63	4.5	4.5	24.32	24.32
2	40.6	3.09	2.19	18.44	13.84	84.99	6.8	5.1	36.75	27.56
3	51.0	3.88	2.75	23.16	17.38	84.99	6.8	5.1	36.75	27.56
4	58.5	4.45	3.15	26.57	19.94	84.99	6.8	5.1	36.75	27.56

The chosen load percentages mimic the situation for typical summer day residential load profile at off-peak hours (i.e. between 4:00 and 6:00 am).

As described previously, a single objective problem to minimize V-f deviations can be achieved by minimizing the steps of Fig. 1. Moreover, the proposed method managed to minimize $|\Delta V_1|$ and $|\Delta f|$ for all steps combined rather than only the first step size. However, in high over-generation mismatch state, the first step of Fig. 1 tends to have high influence on the solution. Therefore, it was chosen to represent V-f deviations result for all investigated cases, as the final settlement values for $|\Delta V_1|$ and $|\Delta f|$ were approaching zero. The obtained results for DL single objective allocation are shown in Table IV. Minimizing $|\Delta f|$ proved to be successful in bringing f_{ss} closer to nominal value from 1.0173 p.u. to 1.0001 p.u. before and after DL allocation. This has significantly improved frequency regulation for the existing active power mismatch of (4.5/3.8) p.u. As for $|\Delta V_1|$ case, the maximum absolute voltage deviation of all buses from their nominal values, known as maximum voltage error (MVE), has increased in comparison with $|\Delta f|$ case for scenario 1. This was attributed to the higher voltages drop from the nominal value mainly at the downstream nodes. The resultant voltage profile for both objectives is illustrated in Fig. 5. The allocation of DL as a single objective problem came at the expense of increased power losses in light of the assumed power mismatch (+36.56% over-generation), since a DL will act as a lagging current addition in a prevailing inductive current network. As expected, total generated apparent power ($\sum S_{Gi}$) increased from (4.72∠35.16° p.u.) for the No DL case to (6.10∠38.14° p.u.) and (5.84∠39.62° p.u.) for the $|\Delta V_1|$ and $|\Delta f|$ respectively.

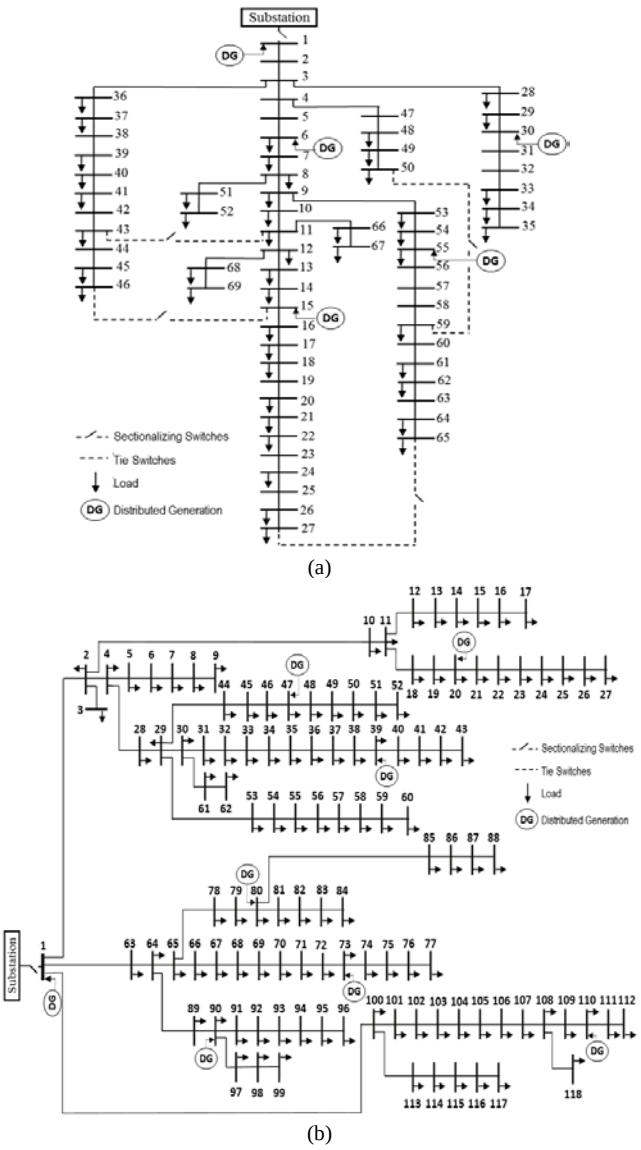

Fig. 5. Test MG single line diagram as modified for autonomous operation: (a) IEEE 69-bus (b) IEEE 118-bus.

This article has been accepted for publication in a future issue of this journal, but has not been fully edited. Content may change prior to final publication. Citation information: DOI10.1109/JSYST.2021.3100409, IEEE Systems Journal

TABLE IV
SINGLE- AND TWO-OBJECTIVES RESULTS FOR SCENARIO 1, 69-BUS SYSTEM

Case	No DL	Min ($\|\Delta V_1\|$)	Min ($\|\Delta f\|$)	Min ($\|\Delta V_1\|$&$\|\Delta f\|$)
Bus No.	-	64	7	27
P_{DL} (p.u.)	-	0.8172	0.6259	0.6294
Q_{DL} (p.u.)	-	0.9999	0.9993	0.9999
$\|\Delta V_1\|$ (p.u.)	0.0480	0.0197	0.0210	0.0208
$\|\Delta f\|$ (p.u.)	0.0170	0.0082	0.0000	0.0005
P_{loss} (p.u.)	0.0578	0.1766	0.0674	0.0880
Q_{loss} (p.u.)	0.0251	0.0710	0.0287	0.0358
MVE (p.u.)	0.0500	0.0366	0.0249	0.0228
f_{ss} (p.u.)	1.0173	0.9920	1.0001	0.9995
Time[a] (s)	-	35	35	40

First step size only for $|\Delta V_1|$ and $|\Delta f|$, [a]algorithm computation time.

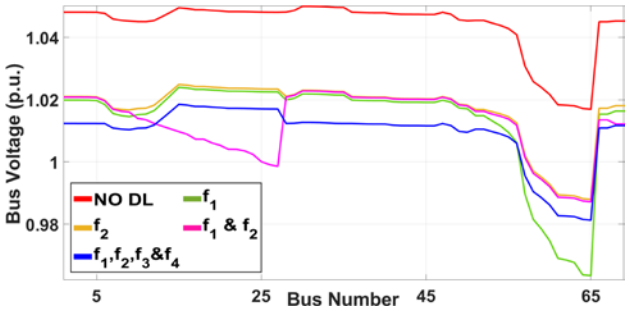

Fig. 5. DL allocation impact on network voltage profile considering different objectives (using Scenario 1, from 69-bus system).

TABLE V
MULTI-OBJECTIVE RESULTS AT DIFFERENT SCENARIOS, 69-BUS SYSTEM

Scenario	1		2		3		4	
Case	No DL	**w/DL**	No DL	**w/DL**	No DL	**w/DL**	No DL	**w/DL**
Bus No.	-	**30**	-	**30**	-	**30**	-	**30**
P_{DL}	-	**0.6580**	-	**0.6253**	-	**0.7781**	-	**0.9332**
Q_{DL}	-	**0.5135**	-	**0.4065**	-	**0.4928**	-	**0.5274**
mn_{DL}	-	**0.0487**	-	**0.0027**	-	**0.0052**	-	**0.0088**
$\|\Delta V_1\|$	0.0480	**0.0123**	0.0779	**0.0014**	0.0626	**0.0019**	0.0515	**0.0024**
$\|\Delta f\|$	0.0170	**0.0003**	0.0985	**0.0016**	0.0767	**0.0021**	0.0609	**0.0023**
P_{loss}	0.0578	**0.0617**	0.0362	**0.0412**	0.0582	**0.0657**	0.0789	**0.0871**
Q_{loss}	0.0251	**0.0255**	0.0174	**0.0170**	0.0271	**0.0272**	0.0359	**0.0360**
MVE	0.0500	**0.0188**	0.0807	**0.0239**	0.0654	**0.0301**	0.0542	**0.0344**
f_{ss}	1.0173	**0.9998**	1.0994	**1.0017**	1.0774	**1.0022**	1.0614	**1.0023**

First step size only for $|\Delta V_1|$ and $|\Delta f|$, all in per unit values

TABLE VI
LOAD FLOW CALCULATION TIME IN SECONDS FOR 69-BUS SYSTEM

Load Flow Method	Using Table I droop with different ε_{Th}[a]				Using mn_{DL} with different scenarios[b]			
	10^{-4}	10^{-8}	10^{-10}	10^{-12}	1	2	3	4
DBFS	0.0152	0.0323	NC	NC	NC	NC	NC	NC
MBFS	0.0051	0.0071	0.0076	0.0086	NC	NC	NC	NC
SBFS	0.0021	0.0026	0.0032	0.0034	0.0025	0.0026	0.0027	0.0029

[a]min ($|\Delta f|$) case only, [b]using $\varepsilon_{Th} = 10^{-8}$, NC: Not Converged.

B. *Multi-Objective Optimization*

A formulation using scenario 1 from the 69-bus system was used for the two-objectives problem, while scenarios 1 - 4 were chosen to represent the generation/load mismatch for the four-objectives problem for both test systems. The PARETOMAX value of the proposed method was set to 1000, while the EPSILON and BALANCE values were set to 0 for all multi-objective cases investigated.

1) Two-objectives optimization

Upgrading the optimization problem into a two-objectives type returned more balanced and satisfactory results with slightly longer calculation time as shown in Table IV. The optimal solution was selected out of many non-dominated solutions based on the utopia-nadir balance approach of the proposed methodology described earlier. Furthermore, this balance of weights can be seen by a better voltage profile with smaller MVE of 0.0228 if compared to the individual objective problems and the No DL case, as illustrated in Fig. 5. Despite that balanced approach to the problem, the solution returned ($5.86\angle 39.53°$ p.u.) of $\sum S_{Gi}$ which did not improve power losses compared to the individual $|\Delta f|$ objective, this could be attributed to the slight increase in the DL power demand as seen in Table IV. However, the advantage of allocating DL in radial distribution systems with high power generation/load ratio was evident in MVE and f_{ss} enhancement. Additionally, the obtained DL locations at buses 64,7 and 27 concur with the idea of random allocations away from a generating bus to help with V-f regulation in the high mismatch situation.

2) Four-objectives optimization

- *69-bus system*

From Table V, upon tackling the many objectives problem the impact of DL allocation on the 69-bus system losses was further reduced. Taking scenario 1 in particular, the $\sum|S_{Gi}|$ obtained of ($5.56\angle 35.57°$ p.u.) was lower if compared to the single objectives of $|\Delta V_1|$ and $|\Delta f|$ for the same scenario, this can be attributed by the addition of droop as a decision variable to optimize DG units output power post islanding. Furthermore, the voltage error of the system has been enhanced by (-0.004) compared to the two objectives problem as seen from Table V and reflected upon the profile of Fig. 5, this level of voltage correction is the maximum to be achieved over the allocated DL range with the assumed mismatch scenario 1. The optimal solution with equally balanced weights for all four-objectives at the centre of the Pareto front is illustrated in Fig. 6(a). Altering the generation/load scenario has further strengthened the significance of DL allocation in a highly penetrated MG using the proposed method. According to results from Table V, the IMG stability has been significantly improved on the expense of minimal extra losses by consuming the excessive residual power. This improvement is realised by better voltage profiles for all investigated scenarios with DL if compared with the No DL case as illustrated in Fig. 7. Likewise, the obtained f_{ss} for all investigated scenarios were within the permissible frequency range (0.996 – 1.004 p.u.) for islanded systems in accordance with IEEE std.1547.

To understand the advantage of SBFS over the existing DBFS and MBFS methods used in [31], a calculation time table for the 69-test system was constructed after obtaining DL values using the SBFS for the $|\Delta f|$ case (using scenario 1) and the four objectives case (using scenarios 1-4). As Table VI shows, the benefit of SBFS was not limited to the faster calculation time, but also in converging to a solution when using mn_{DL} values which would not have been possible without using SBFS.

This article has been accepted for publication in a future issue of this journal, but has not been fully edited. Content may change prior to final publication. Citation information: DOI10.1109/JSYST.2021.3100409, IEEE Systems Journal

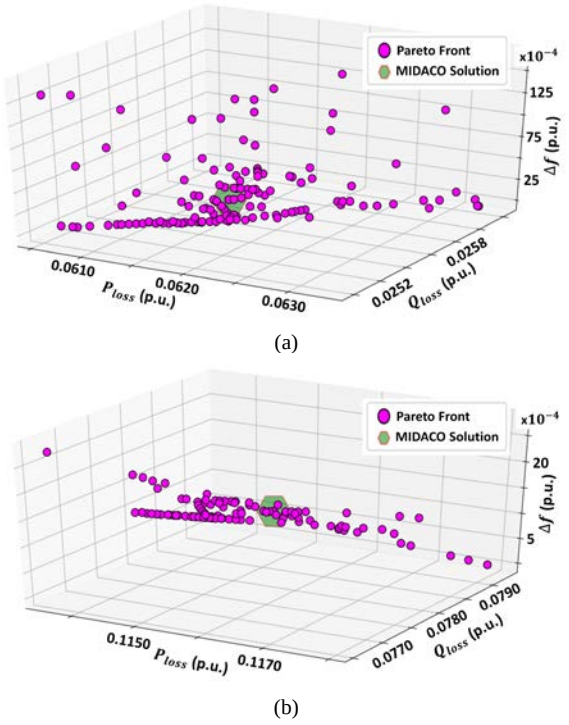

Fig. 6. Four objectives problem Pareto front with zero BALANCE parameter, the optimal solution is highlighted by the hexagon shape at the centre of the pareto front for (a) 69-bus system (b) 118-bus system

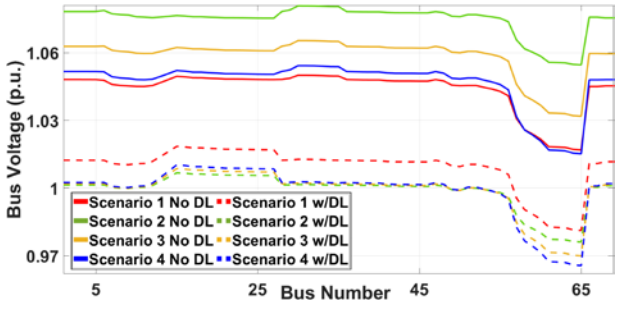

Fig. 7. DL allocation impact on network voltage profile considering different scenarios, 69-bus system.

- *118-bus system*

Expanding the DL allocation problem complexity to a larger system with significant generation capacity and power demand did not deviate from the expected outcome to keep the V-f within acceptable limits. The solution obtained offered balanced results without degrading system losses, while the pareto optimal front of the proposed method is depicted in Fig. 6(b). According to results from Table VII, the location for DL was identical for all scenarios at bus 73 similar to bus 30 for the 69-test system, this might be seen as an efficient and cost-effective application of DL to regulate power variations. Moreover, the resultant voltage profile theme was similar to the 69-test system but with much larger MVE reported as seen in Fig. 8 due to the significant reactive power mismatch (24.32/17.04 over-generation). Furthermore, the latter power mismatch has forced a leading current network situation, which might explain the reduction of losses after the application of DL against the No DL case, similar to an inductive correction procedure in highly capacitive network.

TABLE VII
MULTI-OBJECTIVE RESULTS AT DIFFERENT SCENARIOS, 118-BUS SYSTEM

Scenario	1		2		3		4	
Case	No DL	**w/DL**	No DL	**w/DL**	No DL	**w/DL**	No DL	**w/DL**
Bus No.	-	**73**	-	**73**	-	**73**	-	**73**
P_{DL}	-	**0.4771**	-	**0.3820**	-	**0.4896**	-	**0.5613**
Q_{DL}	-	**0.7289**	-	**0.5860**	-	**0.7293**	-	**0.8467**
mn_{DL}	-	**0.0117**	-	**0.0011**	-	**0.0015**	-	**0.0019**
$\|\Delta V_1\|$	0.1454	**0.0094**	0.2694	**0.0018**	0.1994	**0.0017**	0.1486	**0.0016**
$\|\Delta f\|$	0.0281	**0.0014**	0.3587	**0.0025**	0.2655	**0.0024**	0.1978	**0.0022**
P_{loss}	0.1335	**0.1157**	0.2155	**0.0774**	0.2161	**0.1223**	0.2258	**0.1610**
Q_{loss}	0.0908	**0.0779**	0.1879	**0.0522**	0.1769	**0.0824**	0.1764	**0.1085**
MVE	0.1636	**0.0218**	0.2991	**0.0120**	0.2269	**0.0145**	0.1755	**0.0161**
f_{ss}	1.0301	**1.0015**	1.3687	**1.0026**	1.2722	**1.0025**	1.2025	**1.0023**

First step size only for $|\Delta V_1|$ and $|\Delta f|$, all in per unit values

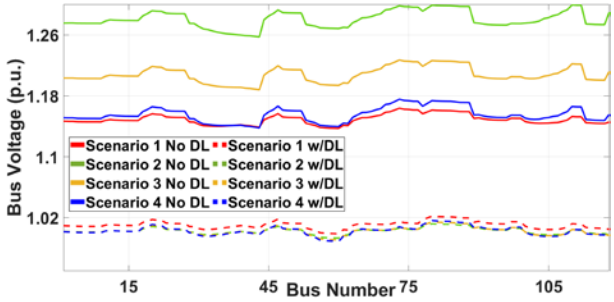

Fig. 8. DL allocation impact on network voltage profile considering different scenarios, 118-bus system.

TABLE VIII
IMPACT OF BALANCE PARAMETER ON THE SOLUTION FOR SCENARIO 1

BALANCE	0	1	2	3	4	0.8411	0.2681	0.6119
Pareto Points	131	11	27	145	220	124	161	222
Bus No.	30	61	25	30	30	30	30	30
P_{DL} (p.u.)	0.6580	0.6579	0.6261	0.6672	0.9319	0.7592	0.6341	0.9886
Q_{DL} (p.u.)	0.5135	0.9999	0.2758	0.5171	0.5425	0.5785	0.4550	0.5795
mn_{DL} (p.u.)	0.0487	0.0001	0.0001	0.0831	0.0848	0.0085	0.0699	0.0652
$\|\Delta V_1\|$ (p.u.)	0.0123	1.5×10^{-5}	3.0×10^{-5}	0.0210	0.0210	0.0020	0.0185	0.0156
$\|\Delta f\|$ (p.u.)	0.0003	2.6×10^{-6}	0	0.0006	0.0051	0.0002	4.0×10^{-5}	0.0047
P_{loss} (p.u.)	0.0617	0.1631	0.0717	0.0606	0.0607	0.0631	0.0609	0.0615
Q_{loss} (p.u.)	0.0255	0.0654	0.0302	0.0250	0.0249	0.0260	0.0252	0.0252

First step size only for $|\Delta V_1|$ and $|\Delta f|$, 69-bus system.

C. *Impact of varying the algorithm parameters*

The solution of the four-objectives problem using scenario 1 from 69-bus system has been tested against variations in the proposed method parameters. Table VIII demonstrates the impact of BALANCE value on the solution, the results show the significance of this parameter and how it alters the focus of the algorithm search effort on the pareto front. Furthermore, the effect of tuning ANTS and KERNEL values has degraded the solution. However, the solution tends to improve when KERNEL value increases as demonstrated in Table IX. The reason behind this improvement is attributed to the influence of K_r in reducing the chances that the algorithm will get stuck in a local minima. The influence of ORACLE parameter on the

This article has been accepted for publication in a future issue of this journal, but has not been fully edited. Content may change prior to final publication. Citation information: DOI10.1109/JSYST.2021.3100409, IEEE Systems Journal

TABLE IX
IMPACT OF ANTS/KERNEL PARAMETER ON THE SOLUTION FOR SCENARIO 1

N_{pop}	K_r	$\|\Delta V_1\|$ (p.u.)	$\|\Delta f\|$ (p.u.)	P_{loss} (p.u.)	Q_{loss} (p.u.)
0	0	0.0123	0.0003	0.0617	0.0255
2	2	0.0136	2 x 10^{-5}	0.0615	0.0255
30	5	0.0127	0.0009	0.0617	0.0254
500	10	0.0128	0.0008	0.0616	0.0254
100	50	0.0109	0.0011	0.0619	0.0255

First step size only for $|\Delta V_1|$ and $|\Delta f|$, 69-bus system.

TABLE X
IMPACT OF ORACLE PARAMETER ON THE SOLUTION FOR SCENARIO 1

Ω	$\|\Delta V_1\|$ (p.u.)	$\|\Delta f\|$ (p.u.)	P_{loss} (p.u.)	Q_{loss} (p.u.)
10^{-3}	0.0250	0.0007	0.0601	0.0248
10^{3}	0.0217	0.0007	0.0605	0.0250
10^{6}	0.0170	0.0005	0.0611	0.0252
10^{9}	0.0123	0.0003	0.0617	0.0255

First step size only for $|\Delta V_1|$ and $|\Delta f|$, 69-bus system.

TABLE XI
IMPACT OF MAXEVAL PARAMETER ON THE SOLUTION FOR SCENARIO 1

MAXEVAL	$\|\Delta V_1\|$ (p.u.)	$\|\Delta f\|$ (p.u.)	P_{loss} (p.u.)	Q_{loss} (p.u.)	Time[a] (s)
500	0.0095	0.0006	0.0633	0.0266	3
1000	0.0129	0.0003	0.0618	0.0256	5
5000	0.0113	0.0004	0.0618	0.0255	21
10000	0.0123	0.0003	0.0617	0.0255	43
20000	0.0123	0.0003	0.0617	0.0255	94

First step size only for $|\Delta V_1|$ and $|\Delta f|$, [a]algorithm computation time, 69-bus system.

TABLE XII
IMPACT OF EPSILON PARAMETER ON THE SOLUTION SCENARIO 1

EPSILON	Pareto Points	$\|\Delta V_1\|$ (p.u.)	$\|\Delta f\|$ (p.u.)	P_{loss} (p.u.)	Q_{loss} (p.u.)	Time[a] (s)
0.01	131	0.0123	0.0003	0.0617	0.0255	43
0.001	708	0.0124	0.0007	0.0617	0.0254	51
0.0001	1000	0.0101	0.0007	0.0620	0.0256	63
0.00001	1000	0.0108	0.0010	0.0619	0.0255	56

First step size only for $|\Delta V_1|$ and $|\Delta f|$, [a]algorithm computation time, 69-bus system.

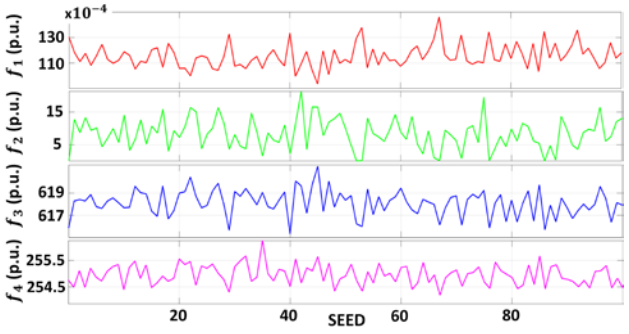

Fig. 9. SEED parameter impact on the solution for the four-objectives problem (Scenario 1, 69-bus system).

solution is shown in Table X, where solution sensitivity of the constrained problem is affected with lower guessed oracles. However, the most reasonable solution was obtained at a sufficiently high oracle equal to the default value of 10^9.

Maximum function evaluation (MAXEVAL) impact on solution fitness is demonstrated in Table XI. The probability of reaching a global optima was increased when MAXEVAL has increased. However, higher values of MAXEVAL beyond 10000 did not further improve the solution. On the other hand, the impact of EPSILON parameter is illustrated in Table XII. As the parameter value decreases the chances becomes higher that new solutions are introduced into the pareto front. However, the calculation time of the algorithm is generally reduced as the value of EPSILON decreased. Lastly, the impact of SEED parameter on the optimal solution of the problem can be realised by looking into Fig. 9. The complexity of the optimization problem was contained by slight difference in optimal solutions generated at different seed, thus eliminating any inconsistency in the results. This in fact changes the optimization approach to the problem from stochastic choice into deterministic global optimization, where the global optimality chance in the obtained overall best solution presented is very high.

D. Comparison with other optimization methods

To further validate the effectiveness of the proposed method, the achieved results were compared with competitive metaheuristics techniques: multi-objective GA (MOGA) [51], the non-dominated sorting GA (NSGA-II) [52], [53], and multi-objective PSO (MOPSO) [54], [55]. The results achieved by each of the three methods are listed in Table XIII for both the 69-&118-bus systems. Tests were carried out using scenario 1 with load model set 1. To simulate the problem using MOGA: population size was 100, probabilities of crossover and mutation were 0.8 and 0.001 respectively. NSGA-II parameters, on the other hand, such as population size, distribution indexes for crossover and mutation, and probability of mutation were 100, 100, 20 and 0.25 respectively. Lastly, MOPSO had a total of 11 parameters: population size 100, repository size 100, cognitive and social learning coefficients 0.1 and 0.2, inertia starting and ending weight 0.5 and 0.001, grid per dimension 7, inflation rate 0.1,

TABLE XIII
COMPARISON WITH OTHER METHODS

Method	MOGA		NSGA-II		MOPSO		MIDACO	
Test System	69	**118**	69	**118**	69	**118**	69	**118**
Bus No.	30	**80**	30	**80**	30	**80**	30	**73**
P_{DL} (p.u.)	0.7741	**0.6505**	0.7985	**0.7219**	0.9031	**0.7183**	0.6580	**0.4771**
Q_{DL} (p.u.)	0.4623	**0.7885**	0.6714	**0.8864**	0.5634	**0.6862**	0.5135	**0.7289**
mn_{DL} (p.u.)	0.0747	**0.0178**	0.0613	**0.0205**	0.0519	**0.0179**	0.0487	**0.0117**
$\|\Delta V_1\|$ (p.u.)	0.0149	**0.0141**	0.0136	**0.0160**	0.0126	**0.0144**	0.0123	**0.0094**
$\|\Delta f\|$ (p.u.)	0.0030	**0.0017**	0.0020	**0.0018**	0.0028	**0.0015**	0.0003	**0.0014**
P_{loss} (p.u.)	0.0617	**0.1152**	0.0617	**0.1146**	0.0618	**0.1152**	0.0617	**0.1157**
Q_{loss} (p.u.)	0.0253	**0.0782**	0.0253	**0.0779**	0.0254	**0.0783**	0.0255	**0.0779**
MAXEVAL	400	**400**	200	**200**	500	**500**	10000	**10000**
Time[a] (s)	235	**397**	922	**1495**	642	**798**	43	**62**

First step size only for $|\Delta V_1|$ and $|\Delta f|$, [a]algorithm computation time.

TABLE XIV
ITERATIONS NUMBER FOR ERROR CONVERGENCE AT DIFFERENT ε_{Th}

Method		No DL	MOGA		NSGA-II		MOPSO		MIDACO	
Test System		69	**118**	69	**118**	69	**118**	69	**118**	69	**118**
ε_{Th}	10^{-4}	42	**NC**	27	**44**	28	**44**	28	**43**	25	**42**
	10^{-6}	55	**NC**	37	**57**	35	**57**	35	**60**	30	**48**
	10^{-8}	75	**NC**	47	**74**	45	**76**	46	**73**	36	**62**
	10^{-10}	97	**NC**	61	**94**	60	**96**	63	**94**	47	**83**

NC: Not Converged.

leader selection pressure 2, deletion selection pressure 2, and mutation rate 0.1. From Table XIII, the 69-bus system results demonstrate that MIDACO outweighs the other three methods in the first two objectives. Furthermore, the obtained losses were similarly close by all four methods. As for the results of the 118-bus system on the other hand, the obtained first objective by MIDACO was much less if compared to the other three methods. Nevertheless, the achieved losses by NSGA-II were the lowest on the expense of higher V-f deviations compared to all other methods. The clear time advantage of the proposed method is demonstrated by getting thousands of function evaluations in much less time if compared with the other methods for both test systems. Speed and accuracy come hand in hand when considering real-time application. This speed shall facilitate real-time operation using the proposed method as described earlier in section 2. Lastly, the proposed method solution efficacy for DL allocation was validated by faster convergence rate in the load flow error at different ε_{Th} for both test systems. This was compared with the No DL case and the other methods solution using scenario 1 for both test systems but adopting load model (set 2) to raise the challenge of getting converged load flow solution for the same problem as shown in Table XIV.

V. CONCLUSION

In this paper, the problem of V-f deviations surpassing their permissible limits in highly penetrated DCIMG during off-peak hours has been addressed. The importance of DL allocation with optimal droop settings has been investigated and validated on 69- and 118-test systems considering different generation/load scenarios. A novel methodology using MIDACO combined with SBFS load flow has been applied to solve the optimization problem in three stages: single-objective to minimize V-f individually, two-objectives problem to minimize V-f simultaneously, and finally a four-objectives problem to minimise V-f, active and reactive power losses. The benefit of the proposed load flow method was shown by better convergence at lower tolerance and droop settings, while the advantage of the proposed optimization method in speed and accuracy was compared and validated with other competitive metaheuristic optimization algorithms. Test results have shown that the proposed method is capable of minimizing V-f fluctuations to comply with IEEE std.1547 for islanded systems while keeping system losses caused by DL application to minimum.

Futurework could be expanded to account for cost of renewable generation curtailment, emissions from conventioanl generation, uncertainties in renewable generation and load demand behaviour change in a highly penetrated DCIMG.

VI. REFERENCES

[1] M. A. Jirdehi, V. S. Tabar, S. Ghassemzadeh, and S. Tohidi, "Different aspects of microgrid management: A comprehensive review," *J. Energy Storage*, vol. 30, p. 101457, Aug. 2020.

[2] M. F. Zia, E. Elbouchikhi, and M. Benbouzid, "Microgrids energy management systems: A critical review on methods, solutions, and prospects," *Appl. Energy*, vol. 222, pp. 1033–1055, Jul. 2018.

[3] S. R. Sinsel, R. L. Riemke, and V. H. Hoffmann, "Challenges and solution technologies for the integration of variable renewable energy sources—a review," *Renew. Energy*, vol. 145, pp. 2271–2285, Jan. 2020.

[4] V. S. Tabar and V. Abbasi, "Energy management in microgrid with considering high penetration of renewable resources and surplus power generation problem," *Energy*, vol. 189, p. 116264, Dec. 2019.

[5] K. Tantrapon, P. Jirapong, and P. Thararak, "Optimal Operation of Battery Energy Storage System for Mitigating Voltage Fluctuation in Microgrid Using Cuckoo Search Optimization," in *Proc. 16th ECTI-CON*, Pattaya, Thailand, 2019, pp. 877–880.

[6] K. S. El-Bidairi, H. D. Nguyen, T. S. Mahmoud, S. D. G. Jayasinghe, and J. M. Guerrero, "Optimal sizing of Battery Energy Storage Systems for dynamic frequency control in an islanded microgrid: A case study of Flinders Island, Australia," *Energy*, vol. 195, p. 117059, Mar. 2020.

[7] R. Rana, M. Singh, and S. Mishra, "Design of Modified Droop Controller for Frequency Support in Microgrid Using Fleet of Electric Vehicles," *IEEE Trans. Power Syst.*, vol. 32, no. 5, pp. 3627–3636, Sep. 2017.

[8] P. Li, W. Hu, X. Xu, Q. Huang, Z. Liu, and Z. Chen, "A frequency control strategy of electric vehicles in microgrid using virtual synchronous generator control," *Energy*, vol. 189, p. 116389, Dec. 2019.

[9] X. Zhu, M. Xia, and H.-D. Chiang, "Coordinated sectional droop charging control for EV aggregator enhancing frequency stability of microgrid with high penetration of renewable energy sources," *Appl. Energy*, vol. 210, pp. 936–943, Jan. 2018.

[10] A. Elrayyah, F. Cingoz, and Y. Sozer, "Smart Loads Management Using Droop-Based Control in Integrated Microgrid Systems," *IEEE J. Emerg. Sel. Top. Power Electron.*, vol. 5, no. 3, pp. 1142–1153, Sep. 2017.

[11] A. Nisar and M. S. Thomas, "Comprehensive Control for Microgrid Autonomous Operation With Demand Response," *IEEE Trans. Smart Grid*, vol. 8, no. 5, pp. 2081–2089, Sep. 2017.

[12] M. Faisal, M. A. Hannan, P. J. Ker, A. Hussain, M. B. Mansor, and F. Blaabjerg, "Review of Energy Storage System Technologies in Microgrid Applications: Issues and Challenges," *IEEE Access*, vol. 6, pp. 35143–35164, May 2018.

[13] M. C. Falvo, G. Graditi, and P. Siano, "Electric Vehicles integration in demand response programs," in *Proc. SPEEDAM*, Ischia, Italy, 2014, pp. 548–553.

[14] C. P. Ion and C. Marinescu, "Autonomous micro hydro power plant with induction generator," *Renew. Energy*, vol. 36, no. 8, pp. 2259–2267, Aug. 2011.

[15] I. Şerban and C. Marinescu, "Aggregate load-frequency control of a wind-hydro autonomous microgrid," *Renew. Energy*, vol. 36, no. 12, pp. 3345–3354, Dec. 2011.

[16] V. Rajagopal, B. Singh, and G. K. Kasal, "Electronic load controller with power quality improvement of isolated induction generator for small hydro power generation," *IET Renew. Power Gener.*, vol. 5, no. 2, pp. 202–213, Mar. 2011.

[17] R. R. Singh, B. A. Kumar, D. Shruthi, R. Panda, and C. T. Raj, "Review and experimental illustrations of electronic load controller used in standalone Micro-Hydro generating plants," *Eng. Sci. Technol. Int. J.*, vol. 21, no. 5, pp. 886–900, Oct. 2018.

[18] P. S. Bhakar, G. K. Rao, and S. Sarangi, "A Novel Adaptive Frequency Control Strategy for Micro Grid," in *Proc. 14th IEEE INDICON*, Roorkee, India, 2017, pp. 1013–1018.

[19] A. Tomar, D. Sharma, and S. Mishra, "An active power management strategy in a microgrid having static and rotating generators considering generation limits using water pumping loads," in *Proc. ICCCE*, Jaipur, India, 2017, pp. 484–488.

[20] T. Caldognetto and P. Tenti, "Microgrids Operation Based on Master–Slave Cooperative Control," *IEEE J. Emerg. Sel. Top. Power Electron.*, vol. 2, no. 4, pp. 1081–1088, Dec. 2014.

[21] X. Hoa Thi Pham, "Power sharing strategy in islanded microgrids using improved droop control," *Electr. Power Syst. Res.*, vol. 180, p. 106164, Mar. 2020.

[22] J.-O. Lee, E.-S. Kim, and S.-I. Moon, "Determining P-Q Droop Coefficients of Renewable Generators for Voltage Regulation in an Islanded Microgrid," *Energy Procedia*, vol. 107, pp. 122–129, Feb. 2017.

[23] M. Džamarija and A. Keane, "Autonomous Curtailment Control in Distributed Generation Planning," *IEEE Trans. Smart Grid*, vol. 7, no. 3, pp. 1337–1345, May 2016.

[24] D. K. Dheer, S. Doolla, S. Bandyopadhyay, and J. M. Guerrero, "Effect of placement of droop based generators in distribution network on small signal stability margin and network loss," *Int. J. Electr. Power Energy Syst.*, vol. 88, pp. 108–118, Jun. 2017.

[25] V. B. Foroutan, M. H. Moradi, and M. Abedini, "Optimal operation of autonomous microgrid including wind turbines," *Renew. Energy*, vol. 99, pp. 315–324, Dec. 2016.

[26] M. H. Moradi, M. Abedini, and S. M. Hosseinian, "Optimal operation of autonomous microgrid using HS–GA," *Int. J. Electr. Power Energy Syst.*, vol. 77, pp. 210–220, May 2016.
[27] C. Chen, S. Duan, T. Cai, B. Liu, and G. Hu, "Optimal Allocation and Economic Analysis of Energy Storage System in Microgrids," *IEEE Trans. Power Electron.*, vol. 26, no. 10, pp. 2762–2773, Oct. 2011.
[28] C. Chen and S. Duan, "Optimal allocation of distributed generation and energy storage system in microgrids," *IET Renew. Power Gener.*, vol. 8, no. 6, pp. 581–589, Aug. 2014.
[29] S. Conti, R. Nicolosi, S. A. Rizzo, and H. H. Zeineldin, "Optimal Dispatching of Distributed Generators and Storage Systems for MV Islanded Microgrids," *IEEE Trans. Power Deliv.*, vol. 27, no. 3, pp. 1243–1251, Jul. 2012.
[30] A. Maulik and D. Das, "Optimal Operation of Droop-Controlled Islanded Microgrids," *IEEE Trans. Sustain. Energy*, vol. 9, no. 3, pp. 1337–1348, Jul. 2018.
[31] A. Uniyal and S. Sarangi, "Optimal allocation of ELC in microgrid using droop controlled load flow," *Transm. Distrib. IET Gener.*, vol. 13, no. 20, pp. 4566–4578, Oct. 2019.
[32] G. Díaz, J. Gómez-Aleixandre, and J. Coto, "Direct Backward/Forward Sweep Algorithm for Solving Load Power Flows in AC Droop-Regulated Microgrids," *IEEE Trans. Smart Grid*, vol. 7, no. 5, pp. 2208–2217, Sep. 2016.
[33] F. Hameed, M. Al Hosani, and H. H. Zeineldin, "A Modified Backward/Forward Sweep Load Flow Method for Islanded Radial Microgrids," *IEEE Trans. Smart Grid*, vol. 10, no. 1, pp. 910–918, Jan. 2019.
[34] M. Schlüter, J. A. Egea, and J. R. Banga, "Extended ant colony optimization for non-convex mixed integer nonlinear programming," *Comput. Oper. Res.*, vol. 36, no. 7, pp. 2217–2229, Jul. 2009.
[35] M. Schlueter and M. Munetomo, "Parallelization strategies for evolutionary algorithms for MINLP," in *Proc. IEEE CEC*, Cancun, Mexico, 2013, pp. 635–641.
[36] M. Dorigo, G. D. Caro, and L. M. Gambardella, "Ant Algorithms for Discrete Optimization," *Artif. Life*, vol. 5, no. 2, pp. 137–172, Apr. 1999.
[37] M. Lopez-Ibanez and T. Stutzle, "The Automatic Design of Multiobjective Ant Colony Optimization Algorithms," *IEEE Trans. Evol. Comput.*, vol. 16, no. 6, pp. 861–875, Dec. 2012.
[38] M. Schlüter and M. Gerdts, "The oracle penalty method," *J. Glob. Optim.*, vol. 47, no. 2, pp. 293–325, Jun. 2010.
[39] M. Schlueter, C. H. Yam, T. Watanabe, and A. Oyama, "Parallelization impact on many-objective optimization for space trajectory design," *Int. J. Mach. Learn. Comput.*, vol. 6, no. 1, p. 9, Feb. 2016.
[40] M. Schlueter, C. H. Yam, T. Watanabe, and A. Oyama, "Many-objective optimization of interplanetary space mission trajectories," in *Proc. IEEE CEC*, Sendai, Japan, 2015, pp. 3256–3262.
[41] "IEEE Guide for Design, Operation, and Integration of Distributed Resource Island Systems with Electric Power Systems," *IEEE Std 15474-2011*, pp. 1–54, Jul. 2011.
[42] "IEEE Guide for Conducting Distribution Impact Studies for Distributed Resource Interconnection," *IEEE Std 15477-2013*, pp. 1–137, Feb. 2014.
[43] Y. Li, H.-D. Chiang, B.-K. Choi, Y.-T. Chen, D.-H. Huang, and M. G. Lauby, "Load models for modeling dynamic behaviors of reactive loads: Evaluation and comparison," *Int. J. Electr. Power Energy Syst.*, vol. 30, no. 9, pp. 497–503, Nov. 2008.
[44] Jen-Hao Teng, "A direct approach for distribution system load flow solutions," *IEEE Trans. Power Deliv.*, vol. 18, no. 3, pp. 882–887, Jul. 2003.
[45] K. Socha, "ACO for Continuous and Mixed-Variable Optimization," in *Proc. 4th Int. Works. (ANTS 2004)*, Brussels, Belgium, 2004, pp. 25–36.
[46] M. Schlueter and M. Munetomo, "MIDACO solver user manual 6.0," Hokkaido University, Sapporo, Japan, Technical Report, 2018. [Online]. Available: http://www.midaco-solver.com/data/other/MIDACO_User_Manual.pdf.
[47] M. E. Baran and F. F. Wu, "Optimal capacitor placement on radial distribution systems," *IEEE Trans. Power Deliv.*, vol. 4, no. 1, pp. 725–734, Jan. 1989.
[48] A. Y. Abdelaziz, E. S. Ali, and S. M. Abd Elazim, "Optimal sizing and locations of capacitors in radial distribution systems via flower pollination optimization algorithm and power loss index," *Eng. Sci. Technol. Int. J.*, vol. 19, no. 1, pp. 610–618, Mar. 2016.
[49] R. Jamil Mahfoud, Y. Sun, N. Faisal Alkayem, H. Haes Alhelou, P. Siano, and M. Shafie-khah, "A Novel Combined Evolutionary Algorithm for Optimal Planning of Distributed Generators in Radial Distribution Systems," *Appl. Sci.*, vol. 9, no. 16, Art. no. 16, Jan. 2019.
[50] Y. M. Atwa and E. F. El-Saadany, "Probabilistic approach for optimal allocation of wind-based distributed generation in distribution systems," *IET Renew. Power Gener.*, vol. 5, no. 1, pp. 79–88, Jan. 2011.
[51] K. Deb, *Multi-Objective Optimization using Evolutionary Algorithms*, vol. 16. Hoboken, NJ, USA: John Wiley & Sons, 2001.
[52] K. Deb, A. Pratap, S. Agarwal, and T. Meyarivan, "A fast and elitist multiobjective genetic algorithm: NSGA-II," *IEEE Trans. Evol. Comput.*, vol. 6, no. 2, pp. 182–197, Apr. 2002.
[53] K. Deb and S. Agrawal, "A Niched-Penalty Approach for Constraint Handling in Genetic Algorithms," in *Proc. ICANNGA*, Portorož, Slovenia, 1999, pp. 235–243.
[54] C. A. C. Coello, G. T. Pulido, and M. S. Lechuga, "Handling multiple objectives with particle swarm optimization," *IEEE Trans. Evol. Comput.*, vol. 8, no. 3, pp. 256–279, Jun. 2004.
[55] M. R. Sierra and C. A. C. Coello, "Improving PSO-Based Multi-objective Optimization Using Crowding, Mutation and ∈-Dominance," in *Proc. 3rd ICEMO*, Guanajuato, Mexico, 2005, pp. 505–519.

Maen Zohair Kreishan received the B.Sc. degree in Electrical Engineering from the University of Jordan, Amman, Jordan in 2009, and the M.Sc. degree in Power Systems and Energy Management from City, University of London, UK in 2014. He is working towards the PhD degree, and is currently with the Department of Electronic and Electrical Engineering, Brunel University London, UK. His research interest include power system modelling, distributed generation control, renewable energy integration, optimization, smart grids, swarm and evolutionary intelligence.

Ahmed Faheem Zobaa (M'02-SM'04) received his BSc (Hons), MSc, and PhD degrees in Electrical Power & Machines from Cairo University, Egypt, in 1992, 1997, and 2002, respectively. He received his Postgraduate Certificate in Academic Practice from University of Exeter, UK in 2010, and his Doctoral of Science from Brunel University London, UK in 2017. He was an Instructor from 1992–1997, a Teaching Assistant from 1997–2002, and an Assistant Professor from 2002–2007 at Cairo University, Egypt. From 2007 to 2010, he was a Senior Lecturer in renewable energy at University of Exeter, UK. From 2010 to 2019, he was a Senior Lecturer in power systems at Brunel University London, UK. He is currently a Reader in electrical and power engineering at Brunel University London, UK. His main areas of expertise include power quality, (marine) renewable energy, smart grids, energy efficiency and lighting applications.